STRUCTURAL OPTIMIZATION DESIGN OF JET COOLING DEVICE FOR LITHIUM BATTERIES OF NEW ELECTRIC VEHICLES

Zhendong ZHANG[1], Xinjian LI[2], Shanshan PENG[3]*

Aiming at the problem of excessive heat output caused by the lithium battery rapid charging technology used in electric vehicles, an immersed array jet cooling device was designed. The nozzle diameter, jet height, transverse and longitudinal jet spacing were taken as test factors, The maximum temperature, temperature difference, system pressure loss and Nu value on the jet impact surface were taken as evaluation indexes. The orthogonal test was designed and completed. Fluent software was used to simulate the jet cooling process of the device, and the optimal horizontal and vertical nozzle spacing was obtained through particle swarm optimization algorithm. The influence trend of the optimized spacing before and after the optimization on the overall flow field fluidity was analyzed combined with the flow velocity cloud image, The cooling effect of the optimal spacing was verified by the array jet cooling experimental platform. The optimization design of jet cooling device for electric vehicle lithium battery is performed.

Keywords: Jet cooling, numerical simulation, particle swarm optimization, array jet cooling experimental.

1. Introduction

With the increasing electric density of lithium batteries and the gradual increase in the number of battery packs in the electric box, new electric vehicles are at risk of spontaneous combustion accidents during driving, parking and charging. Lithium battery fire will not only damage the car, but also cause casualties in serious cases. However, the development of new electric vehicless needs to be supported by high electric density lithium batteries and fast charging technology, which undoubtedly requires high cooling efficiency of the cooling device. Therefore, it is of great significance to study the cooling device of new electric vehicles lithium battery [1].

Singh et al. [2] used a encapsulated disguised change phase material (PCM) combined with a forced convection air cooled battery thermal management system (BTMS) proposed a coupled electrochemics-thermal model and established simple predictive correlations for a prior estimate of mean and

[1] Prof., Mechanical engineering, Anhui Institute of Information Technology, China, e-mail: 2016048@aiit.edu.cn
[2] MR., Anhui Polytechnic University, China, e-mail: 2190130115@stu.ahpu.edu.cn
[3]* Prof., Mechanical engineering, Anhui Institute of Information Technology, China, e-mail: 2013052@aiit.edu.cn

maximum battery temperatures in the color gamut of the relevant parameters. Talele et al. [3] optimized the PCM battery pack structure and concluded that the design has the dual function of delaying the cell thermal runaway trigger point and slowing the heat propagation by at least 800 seconds. Thakur et al. [4] summarized the latest advances in thermal management of advanced lithium-ion batteries with high charge-discharge cycles, and detailed existing advanced of BTMS from the point of view of fast charge-discharge rates. Kirad K et al. [5] studied the effect of variation in the transverse and longitudinal spacing between lithium batteries on each evaluation parameter and established a numerical model of the battery module cooling system for analyzing the system, concluding that the transverse spacing had a significant effect on the cooling efficiency, while the longitudinal spacing had a significant effect on the temperature uniformity. Kaood A et al. [6] introduced a compact and efficient millimeter-scale jet impingement cooling module, which was numerically simulated using Fluent, and the results of the study showed that it was effective to improve the cooling efficiency by controlling the flow structure under restricted flow. Ruhani B et al. [7] simulated the cooling system of lithium battery, explored the pressure drop and temperature variation of the cooling system by changing the size of the coolant inlet and outlet and the Reynolds value of the system, and concluded that the increase of the Reynolds value and the size of the inlet will intensify the pressure drop in the cooling system. Li et al. [8] used the z-fraction method to numerically simulate and analyze six types of cooling plate designs under different inlet flow rates, in order to evaluate the impact of cooling plate layout and channel design on the heat dissipation of battery modules, and concluded that the comprehensive performance of the cooling plate with multiple small flow channels was optimal. Mehmandoosti et al. [9] used Strouhal value, oscillation amplitude and Reynolds value as characteristic parameters to explore the effect of parameter variation on the maximum temperature and maximum temperature difference of the system, and the optimal combination of parameters was obtained by using artificial intelligence model for bi-objective optimization. Garg A et al. [10] used pitch size, inlet velocity and inlet temperature of the outermost channel as battery cooling system design parameters and used Thompson sampling efficient multi-objective optimization algorithm to obtain the best system cooling results. Duan et al. [11] conducted a numerical study on the three-dimensional temperature distribution of the battery liquid cooling system, and studied the influence of channel size and inlet boundary conditions on the temperature field of the battery module. Shahid [12] used cylindrical batteries as the cooling object and air as the cooling medium. The research results showed the introduction of multiple delta wing vortex generators to enhance turbulence before the interaction between the airflow and porous surfaces, in order to enhance heat transfer. In summary, the current research of relevant scholars mainly focuses on the optimization of battery

cooling systems, involving various cooling technologies and battery module design, including traditional forced convection, phase change materials, coolant flow characteristics and cooling plate structure design. With a focus on increasing cooling efficiency, reducing temperature differences and improving thermal management performance, this paper continues to explore how to improve the overall performance and adaptability of the cooling system through different optimization methods, such as numerical simulation and multi-objective optimization algorithms. However, the application of submerged jet cooling technology is less discussed, and it is difficult to provide refined and targeted solutions to the cooling problem of lithium batteries.

In the present study, a new electric vehicle submerged array jet cooling device is designed based on the size of 18650 lithium battery. The heat transfer and flow characteristics of jet cooling are simulated by using Fluent with deionized water as the cooling medium. The nozzle diameter, jet height, transverse and longitudinal jet spacing are selected as the influencing factors, and the maximum temperature, temperature difference, system pressure loss, and Nu value on the jet impact surface are selected as evaluation indicators. To design and complete the orthogonal test, the main factor affecting the cooling effect when $H/D = 1$ is the transverse and longitudinal jet spacing, the range analysis has been used. To obtain the optimal spacing at $H/D = 1$ by particle swarm optimization algorithm, the trend of the influence of the spacing value on the overall flow field fluidity before and after optimization is analyzed by combining with the flow velocity cloud chart. The array jet cooling experimental platform is built to verify the cooling effect of the optimal spacing value, the design and optimization of jet cooling device for lithium batteries of new electric vehicles.

2. Design of jet cooling system for new electric vehicles

The conventional air cooling system has a simple structure and poor heat exchange effect, which is not enough to cope with the future high electric density power battery pack. At this stage, most of the indirect liquid cooling method is used, and there is the disadvantage of uneven temperature distribution of the power battery pack [13].

The structure diagram of the jet cavity is shown in Fig. 1, and the jet generating device consists of the jet cavity and nozzles. The cooling medium enters the jet cavity from the storage tank through a cooling water pump, stabilizes the pressure and flow, and is then sprayed out through the jet holes. The high-speed jet flows to the heat dissipation expansion copper plate of the lithium battery pack for heat dissipation, and the coolant flows back to the reservoir through the outlet after completing the heat exchange [14]. The nozzle array is distributed in the jet cavity, with transverse and longitudinal jet spacing of L_1 and

L_2 respectively, and the jet height is expressed as H, the nozzle length l is 25 mm, and the nozzle diameter D is 10 m.

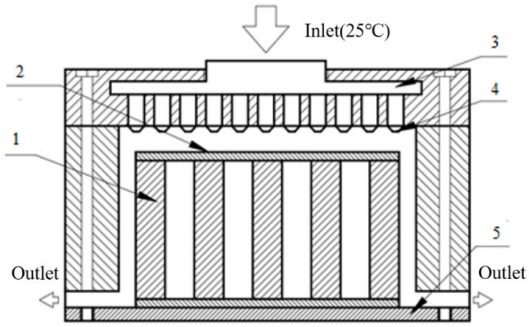

Fig. 1. Structure diagram of jet cavity
1- Lithium battery 2- Heat dissipation expansion copper plate 3- Jet cavity 4- Jet hole 5- Device base

3. Numerical simulation of jet cooling based on orthogonal test optimization

3.1 Modeling of device structure and analysis of model mesh independence

The numerical simulation of jet cooling only considers the flow characteristics of the coolant in the box and the heat transfer characteristics in the heat exchange process, without considering other influencing factors such as stress and strain of the device in the cooling process. As shown in Fig. 2, the established model reduces the number of nozzles and only the cooling effect of the middle two rows of nozzles is studied and analyzed in the numerical simulation.

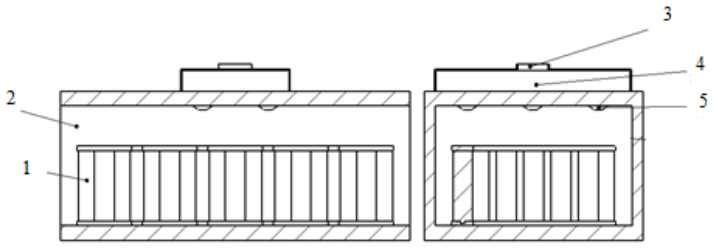

Fig. 2. Simplified diagram of jet cavity
1- Lithium battery 2- Coolant outlet 3- Coolant inlet 4- Jet cavity 5- Jet hole

As shown in Fig. 3, the complex flow field situation of the jet cavity, jet hole and jet impact surface in the fluid region requires encryption of the mesh and the use of unstructured mesh to increase its computational accuracy. Also, since the heat dissipation expansion copper plate in the solid region belongs to the jet

heat transfer surface, it is also necessary to encrypt the mesh, and the rest of the solid wall region is an adiabatic part not involved in the jet heat transfer, using a larger size of hexahedral mesh [15]. The grid of its fluid domain and box is shown in Fig. 4 and Fig. 5.

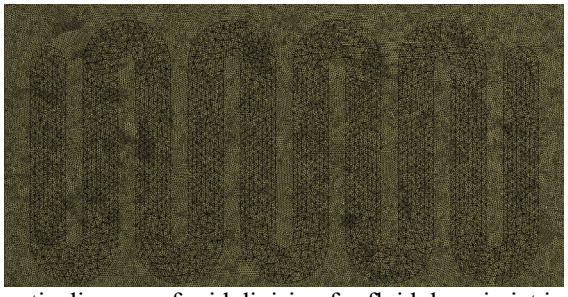

Fig. 3. Schematic diagram of grid division for fluid domain jet impact surface

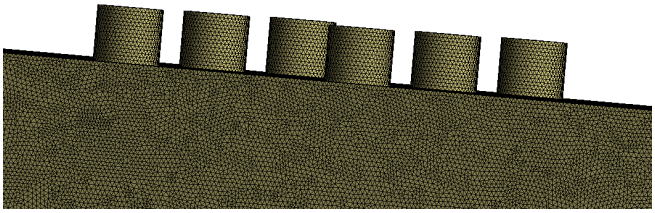

Fig. 4. Grid diagram of fluid domain

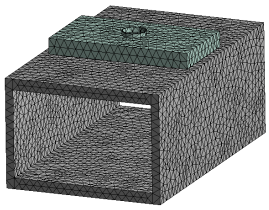

Fig. 5. Grid diagram of box

3.2 Numerical simulation of jet cooling based on orthogonal experimental design

In this paper, the nozzle diameter, jet height, transverse and longitudinal jet spacing are selected as the influencing factors, and three levels are evenly selected for each factor, and the maximum temperature, temperature difference, system pressure loss, and Nu value on the jet impact surface are selected as evaluation indicators. The effect of each structural parameter on the cooling process of the jet is investigated by orthogonal tests, and the experimental factors and level quantities are divided as shown in Table 1 [16].

Table 1

Table of horizontal factor settings

Factors	Level 1	Level 2	Level 3
A Nozzle diameter/mm	9	10	11
B Jet height/mm	8	10	12
C Transverse jet spacing/mm	40	45	50
D Longitudinal jet spacing/mm	30	32	34

Fluent is used for simulation, with the jet flow velocity at the inlet of the jet cavity of 1.5 m/s, the initial temperature of 25 °C, the outlet condition is pressure outlet, the wall is a constant heat flow boundary at the bottom, the heat flow density of 68500 W/m^2, the other wall surfaces are adiabatic, and the jet

impact surface is a fluid-solid coupling surface without slip. The SIMPLE algorithm is used to solve the control equation, and the Second Order Upwind format is used for other calculation models, and the iteration residual is less than 10-6 to determine convergence [17]. The orthogonal test principle is applied to establish the $L_9(3^4)$ orthogonal experiment table, and the simulation analysis is carried out for 9 sets of process parameter combinations. The results are shown in Table 2.

Table 2

Experimental design and results

Number	Factors				Indexes			
	A/mm	B/mm	C/mm	D/mm	T_{max} /℃	ΔT /℃	$\Delta P/Pa$	Nu
1	9	8	40	34	33.27	7.13	75467.41	1058
2	9	10	45	32	32.80	6.78	76059.85	1062
3	9	12	50	30	32.83	6.34	75018.53	1076
4	10	12	45	30	33.23	6.74	77378.90	1052
5	10	8	50	34	32.30	5.84	76564.56	1045
6	10	10	40	32	32.70	6.73	77798.17	1057
7	11	8	50	32	33.20	6.92	80364.43	1027
8	11	10	40	30	32.90	6.30	81166.62	1093
9	11	12	45	34	33.52	6.77	81401.33	1044

The simulation results of 9 sets of jet heat transfer are shown in Fig. 6.

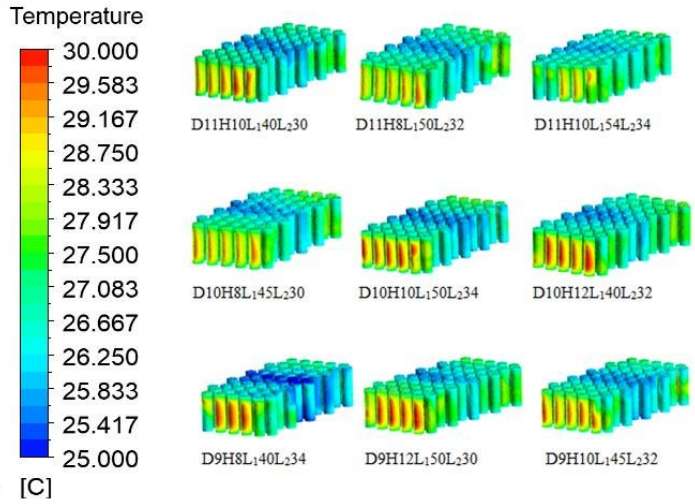

Fig. 6. Chart of temperature distribution in numerical simulation of each group

Using range analysis method to explore the degree of influence of various factors on the maximum temperature of feature points, as shown in Table 3, the range values of each factor are $R_B > R_A > R_C > R_D$, that is, the order of influence

of each factor on the maximum temperature: Jet height > Nozzle diameter > Transverse jet spacing > Longitudinal jet spacing.

Table 3

Range analysis table for maximum temperature

Range	Factors			
	A	B	C	D
K_1	98.90	99.70	98.87	99.10
K_2	98.23	98.00	99.55	98.07
K_3	99.62	99.05	98.33	98.96
k_1	32.97	33.23	32.96	33.03
k_2	32.74	32.67	33.19	32.69
k_3	33.21	33.02	32.78	32.97
R	0.46	0.55	0.41	0.06

Using the above data to create Fig. 7, the best combination of influencing factors can be directly obtained by analyzing the range of the maximum temperature. When the parameter combination is $A_2B_2C_3D_2$, the maximum temperature is the minimum.

The above method is used to analyze the influence degree of each parameter on temperature difference of feature points, system pressure loss of feature points and Nu value on the jet impact surface of feature points, and the data analysis chart is obtained. The best parameter combination can be obtained as $A_2B_2C_3D_3$, $A_1B_3C_3D_1$ and $A_1B_2C_1D_3$ respectively.

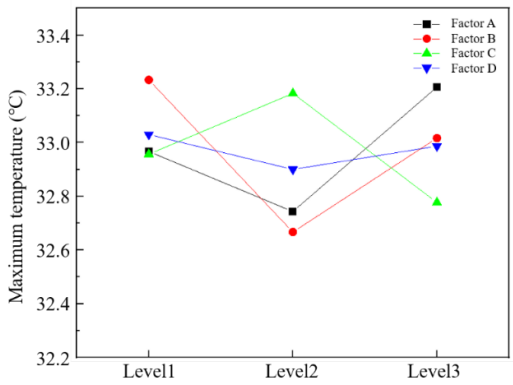

Fig. 7. Range analysis of highest temperature

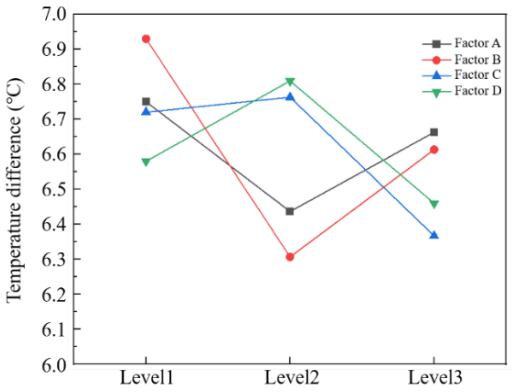

Fig. 8. Range analysis of temperature difference

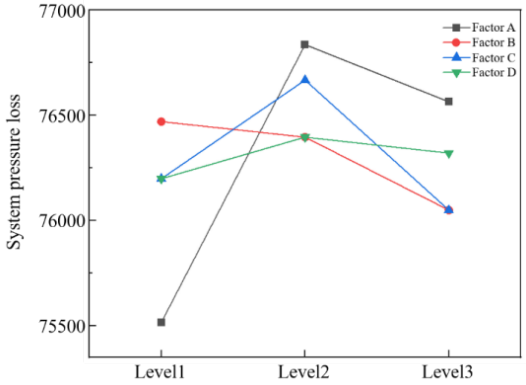

Fig. 9. Range analysis of system pressure loss

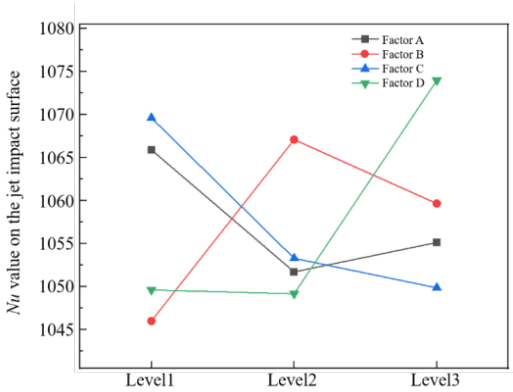

Fig. 10. Range analysis of Nu value on the jet impact surface

From the above optimal parameter combinations, except that the jet height in the system pressure loss is not 10 mm, and the jet height has a minor impact on the system pressure loss, it can be determined that the jet height is 10 mm. Meanwhile, when the transverse jet spacing is in the range of 34 to 50 mm and the longitudinal jet spacing is 34 mm, the maximum temperature and temperature difference values on the feature points are the minimum, and the Nu value is the maximum. Thus, without considering the effect of system pressure loss, the optimal structural parameters can be roughly determined as H = 10mm, D = 10mm, transverse jet spacing range from 34 to 50 mm, and longitudinal jet spacing of 34 mm.

4. Optimization of array jet spacing parameters based on particle swarm algorithm

The first step in this optimization is to establish the functional relationship between the objective function $f(x)$ and the lateral and longitudinal spacing L_1 and L_2 of the nozzle, and then determine the constraints and use optimization methods to optimize the objective.

In heat transfer, the characteristic number equation refers to the relationship between various parameters in convective heat transfer expressed using Nu. Equation 1 is the correlation equation for convective heat transfer of a single jet under a flat plate.

$$Nu = 0.664Re^{1/2}Pr^{1/3} \tag{1}$$

Where Re is Reynolds number; Pr is Prandtl number.

The calculation formula for Reynolds number Re is shown in equation 2:

$$Re = \frac{vd\rho}{u} \tag{2}$$

Where v is characteristic velocity, m/s; d is characteristic radius; ρ is fluid density; u is Fluid dynamic viscosity.

The fitness function graph is commonly used in optimization algorithms to represent the fitness of different solutions. The horizontal axis in the graph usually represents different solutions or variables in the solution space, while the vertical axis represents the fitness value of the corresponding solution. The higher the fitness value, the better the solution. The particle swarm optimization algorithm uses two particles with a maximum number of iterations of 100, as shown in Fig. 11, and the algorithm has completed convergence in about 60 generations [18]. The optimized result is the transverse jet spacing L_1 of 42.6 mm and the longitudinal jet spacing L_2 of 34 mm.

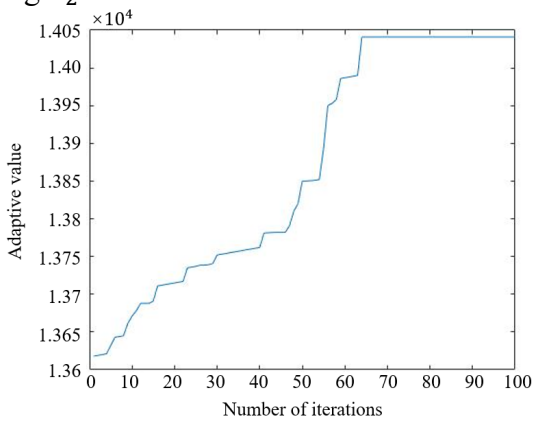

Fig. 11. Particle swarm optimization iteration diagram

The fitness values of each combination of transverse and longitudinal jet spacing are shown in Table 4, where numbers 1 to 9 are the fitness values of three combinations of transverse and longitudinal jet spacing parameters, and numbers 10 are the values obtained through optimization algorithm.

Table 4

Table of fitness Values

Number	Combination(L_1,L_2)	Fitness Value
1	(40,30)	168
2	(45,30)	507
3	(50,30)	1199
4	(40,32)	271
5	(45,32)	5544
6	(50,32)	436
7	(40,34)	754
8	(45,34)	284
9	(50,34)	448
10	(42.6,34)	34671

In order to verify whether the optimized transverse and longitudinal jet spacing parameters can achieve better heat transfer effect, three groups of parameters with greater fitness (50, 30), (45, 32) and (40, 34) are selected as reference groups, and the optimized transverse and longitudinal jet spacing parameters are compared with the three reference groups for jet cooling simulation. After numerical simulation of four sets of jet cooling parameters with different transverse and longitudinal spacing, the temperature values at each feature point can be obtained through CFD-Post post-processing, as shown in Fig. 12 and Fig. 13.

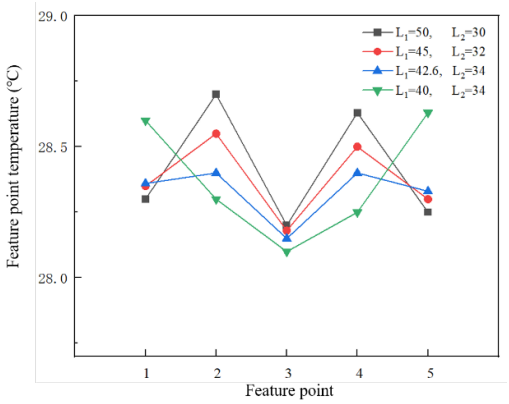

Fig. 12. Temperature of the upper plate

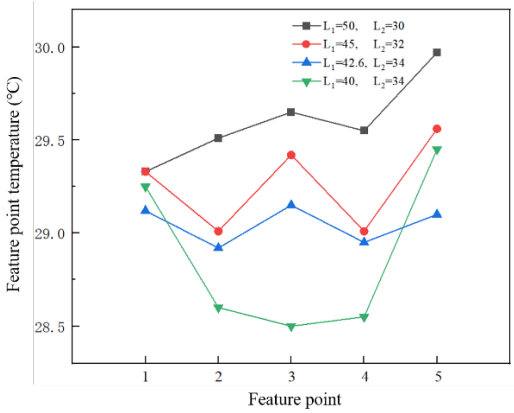

Fig. 13. Temperature of the lower plate

Fig. 12 shows that as the transverse jet spacing decreases, the temperatures of feature points 1 and 5 increase sequentially, while the temperatures of feature points 2 and 4 decrease with significant differences. When the spacing decreases to 40 mm, excessive concentration of the nozzle can cause a large negative pressure in the middle of the flow field, resulting in a decrease in overall flow performance. Fig. 13 shows that the temperature at each point decreases as the transverse spacing decreases. When the transverse spacing decreases to 40 mm, the temperature at feature points 2, 3, and 4 decreases significantly. However, the temperature values at points 1 and 5 on both sides are higher, resulting in a larger overall temperature field temperature difference.

In summary, the region below the jet holes has a lower temperature compared to the region between the jets. The temperature at points 1, 3, and 5, which are directly impacted by the jets, is the lowest. The temperature at points 2 and 4 is influenced by the upward flow generated between the two jet nozzles due to the negative pressure. Smaller transverse spacing results in faster upward flow velocity, leading to better cooling at points 2 and 4. However, when the transverse spacing decreases to a certain value, a larger negative pressure is generated in the intermediate flow field, resulting in poorer overall flow characteristics and larger temperature differences.

To better understand the immersion array jet cooling mechanism, a plane is established in the flow field at a distance of 12 mm from the jet holes. Fig. 14 shows flow velocity cloud chart for the three sets of transverse and longitudinal spacings. The black square in the figure represents the position directly below the jet holes. In case (a), the coolant flow tends to move towards the left side, while in cases (b) and (c), the flow distribution is more uniform. However, compared to case (b), the flow of coolant in the middle region of case (c) exhibits better flow characteristics.

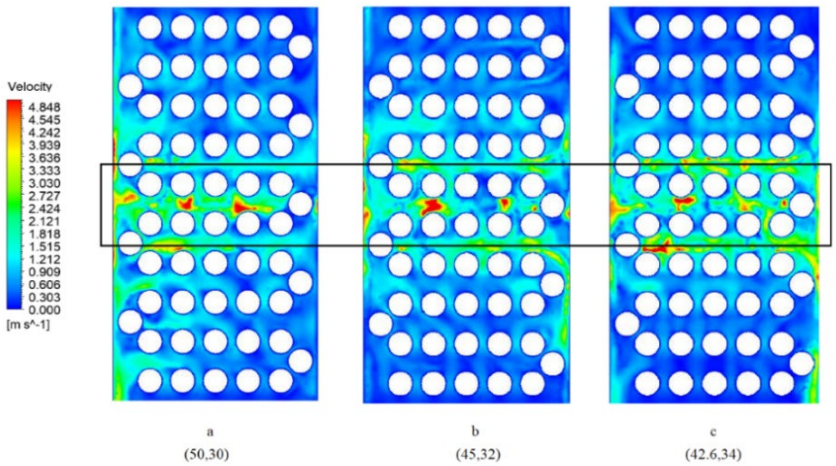

Fig. 14. Flow velocity cloud chart

Based on the relationship between upward flow and jet spacing, it is known that a larger spacing value leads to a lower upward flow velocity and poorer heat transfer efficiency between the jet holes. However, the transverse and longitudinal spacings need to be discussed separately. Considering Fig. 15, when increasing the transverse jets spacing, the impact area of the jets increases due to the heat dissipation expansion copper plate, making it easier to generate upward flow. On the other hand, in the longitudinal direction, the spacing between the rows of lithium batteries affects the jet impact height, reducing the upward flow velocity. Therefore, increasing the longitudinal spacing of the jet holes promotes a more uniform flow field.

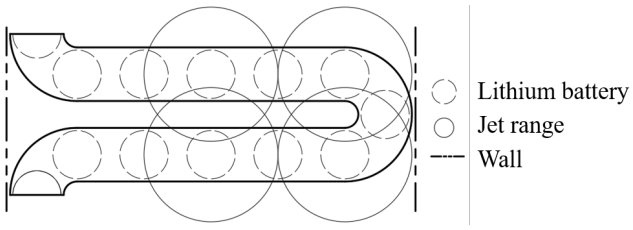

Fig. 15. Jet range diagram

In conclusion, when designing an array jet system, it is advisable to reduce the transverse spacing between the jet nozzles while increasing the longitudinal spacing. The optimized transverse and longitudinal spacing values obtained through particle swarm optimization also align with the aforementioned principles.

5. Array jet cooling experiment

To validate the influence of parameters related to the transverse and longitudinal jet spacing on the optimized cooling effect, a liquid-immersed array jet experimental apparatus with different spacing is designed and constructed. The experimental setup is used to compare the cooling efficiency of three different spacing configurations of the jet holes and to discuss the heat transfer characteristics [19].

5.1 Design and construction of experimental platform

Fig. 16 illustrates the schematic diagram of the jet experiment system. Deionized water is used as the cooling medium, driven by a DC brushless cooling water pump. The temperature of the test specimen is measured using a temperature sensor, and the flow rate is controlled by the control cabinet. The experimental apparatus consists of cooling water pump, constant temperature water tank, control cabinet, DC stabilized power supply, water tank, jet plate, heating plate, and temperature sensor [20].

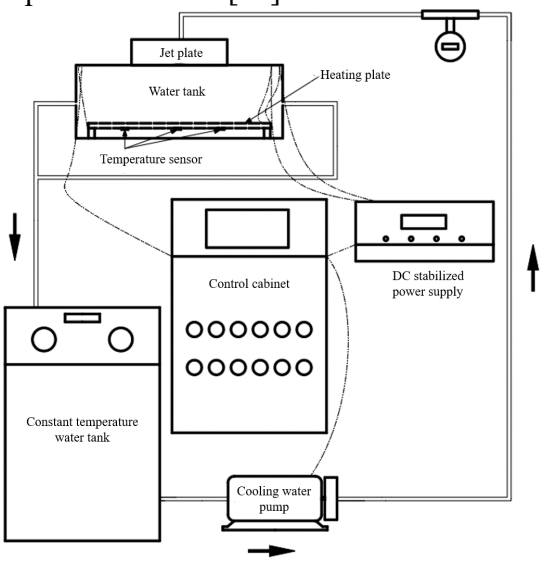

Fig. 16. Jet experiment system diagram

The working principle of the experimental apparatus is as follows: the control cabinet regulates the flow rate of the cooling water pump. The coolant is drawn from the constant temperature water tank (at 25 °C) and delivered into the

jet chamber through the cooling water pump. It then passes through the jet holes and cools the heating plate in the water tank. A temperature sensor is installed at the bottom of the heating plate in the water tank to record the real-time temperature. The liquid crystal display of the control cabinet shows the current flow rate of the cooling water pump and the temperature of the heating plate. After cooling, the coolant flows back to the constant temperature water tank through the return pipe and continues circulating.

As shown in Fig. 17, a heated plate covered with an insulation coating is used in this experiment. The parameters of the heating plate are 300 mm × 180 mm, power of 220 W, thickness of 1.5 mm. The internal surface is coated with carbon fiber spray, with yellow strips on both sides serving as electrodes. The external surface is enveloped with an insulation coating to allow the heating plate to be immersed in water. This heating plate has a fast temperature rise and uniform heat distribution. As shown in Fig. 18, due to the shape and thin thickness of the heating plate, surface-mounted sensors are chosen for their high data accuracy and ease of attachment to the heating plate. The temperature sensor is attached to the bottom of the heating plate, with the sensor surface placed against the bottom surface. The wiring junction is sealed with adhesive silicone gel for waterproofing. The front side of the heating plate faces upwards towards the temperature measurement points through the jet holes.

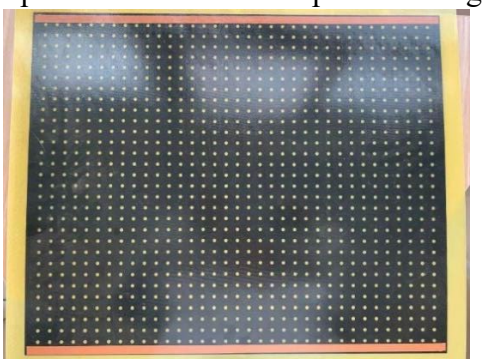

Fig. 17. Internal structure of heating plate

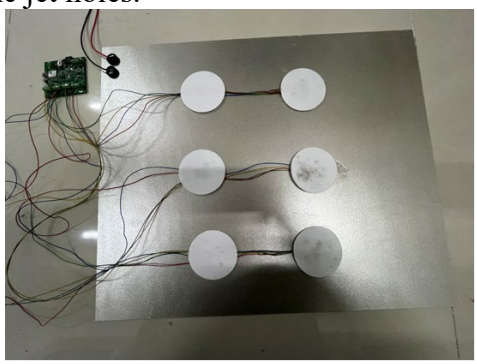

Fig. 18. Sensor distribution diagram

As mentioned in Section 4, the best jet effect is observed when the longitudinal jet spacing is 34 mm. Since the heating plate is a smooth and thin surface without any vertical height difference, a uniform longitudinal spacing is adopted to ensure the accuracy of the experimental validation. Three different transverse jet spacing configurations are designed for comparison. The transverse and longitudinal spacing parameters of the control group's jet plate are (50, 34) and (45, 34) respectively. The entire jet experimental setup, as shown in Fig. 19, consists of a water tank and a jet generation device made of transparent acrylic plates with a thickness of 8 mm. The plates are assembled using adhesive

bonding, and the joints and gaps are sealed with waterproof glass adhesive. Polyurethane foam filler is used to reinforce the joints.

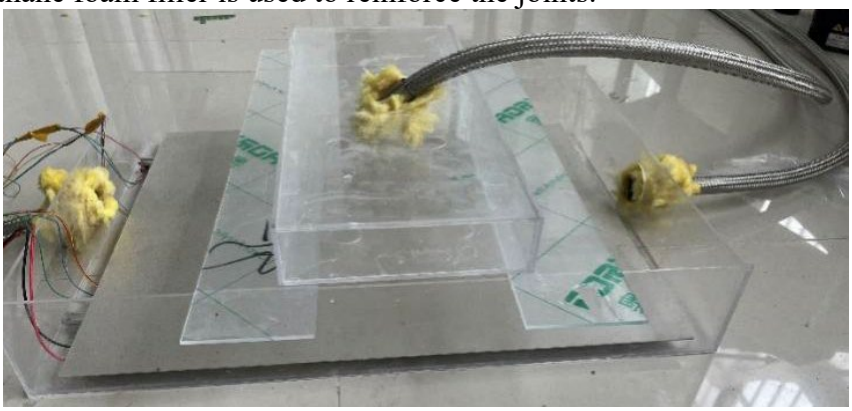

Fig. 19. Jet cooling experimental bench

5.2 Analysis of array jet cooling experimental results

According to the parameters of the jet plate in this experiment, they are respectively (50, 34), (45, 34), and (42.6, 34). The jet height is $H = 10mm$, and the nozzle diameter is $D = 10mm$. Since the longitudinal spacing is consistent, the transverse spacing L_1 and the nozzle diameter D are made dimensionless. By comparing the results of experiments with $L_1/D = 5$, $L_1/D = 4.5$, and $L_1/D = 4.26$, the heat transfer characteristics of the jet cooling device in this experiment can be analyzed.

Fig. 20 shows the variation of the average Nusselt number Nu_b with the Re during the cooling process. A higher Nu_b indicates a stronger heat transfer process [21]. It can be observed from the graph that when $L_1/D = 4.26$, at the same Re, the Nu_b is higher than the other two jet spacing configurations. At the same time, for $Re < 1100$, the Nu_b of the three jet spacing configurations exhibits a linear increase with the Re. For $Re > 1100$, it can be observed that the Nu_b increment of the $L_1/D = 4.26$ configuration starts to decrease.

At $Re = 1385$, the Nu_b of the three jet spacing configurations are essentially the same. This is because when the flow velocity reaches a certain value, with the increase in jet spacing, the jets produced by the holes near the wall collide with the wall surface, forming negative pressure cavities near the heated plate surface and the wall. This intensifies the complexity of the entire flow field, enhances the heat transfer process, and improves the overall heat transfer performance of the device.

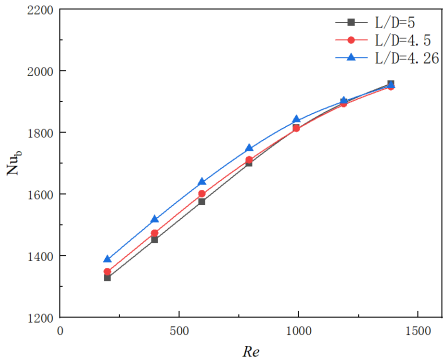

Fig. 20. The trend of Nu_b changing with Re

The Nu_b reflects the overall heat transfer performance, while the local cooling effectiveness needs further analysis. Table 5 presents the temperature values of different monitoring points under various transverse spacings and flow rates.

Table 5

Temperature values of each feature point

Feature point	L_1/D	5	4.26	5	4.26	5	4.26
	Q	0.5	0.5	3	3	1.5	1.5
1		30.98	31.11	28.83	29.11	29.83	29.98
2		31.31	31.18	29.41	29.41	30.24	30.18
3		30.91	30.85	29.22	29.18	29.91	29.89
4		31.29	31.18	29.47	29.41	30.28	30.18
5		31.00	31.09	28.89	29.17	29.9	30.09

Fig. 21 indicates that at low flow velocities, the temperature distribution of the monitoring points shows a trend of being low in the middle and high at both ends. Under the same low flow velocity conditions, the temperatures at points 2 and 4 for $L_1/D = 4.26$ are better than those for $L_1/D = 5$. Although the temperatures at points 1 and 5 are slightly higher than those for $L_1/D = 5$, the overall temperature uniformity is better, and the temperature at point 3 is slightly lower than that for $L_1/D = 5$. As the flow rate increases, the temperature difference between points 2 and 4 in the two different transverse spacing experiments decreases due to the boundary effect of the confined jets. Especially when the flow rate $Q = 3L/min$, the influence of the boundary effect is particularly evident from the graph. Under strong boundary effects, the temperature at point 3 is no longer the lowest among the five points. The strong negative pressure generated near points 1 and 5 on both sides disrupts the boundary flow, thereby enhancing the heat transfer effectiveness.

Fig. 20 has already indicated that at high flow rates, the transverse jet spacing has no significant influence on the overall heat transfer intensity. However, from Fig. 21, significant temperature differences are observable at different measurement points on the heated plate under high flow rates. Moreover,

high flow rates increase the cooling power consumption. Therefore, selecting an appropriate transverse spacing can ensure cooling uniformity and reduce power consumption.

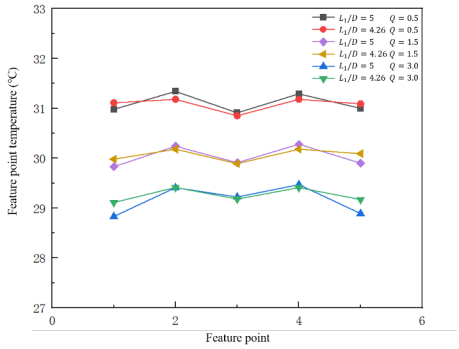

Fig. 21. Temperature of feature points under different flow rates and spacing

Based on the analysis above, when $L_1/D = 4.26$, under low flow rate conditions, its heat transfer performance is better than other parameters. Combining the conclusions drawn earlier, although increasing the flow rate can further reduce the cooling temperature, the negative effects it brings also need to be considered. Therefore, blindly increasing the flow rate to achieve better heat transfer effectiveness is not advisable. The appropriate flow rate can not only reduce pump power consumption but also minimize negative impacts.

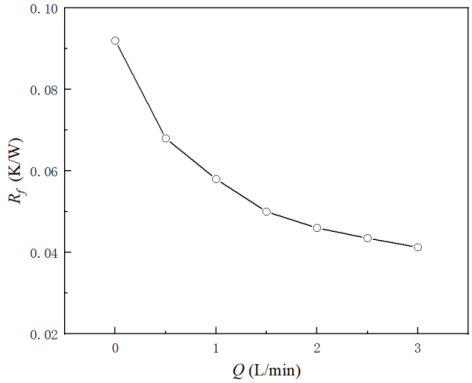

Fig. 22. The trend of R_f changing with Q ($L_1/D = 4.26$)

Fig. 22 shows the variation of thermal resistance with flow rate when $L_1/D = 4.26$. As the flow rate increases, the thermal resistance gradually decreases. However, when the flow rate reaches $1.5L/min$ and continues to increase, the trend of decreasing thermal resistance becomes less significant. This indicates that increasing the flow rate can enhance heat transfer to a certain extent, but the trend of enhanced heat transfer becomes less pronounced after reaching a certain level. Therefore, for the experimental conditions in this study, a flow rate of $1 - 1.5L/min$ is the most suitable choice.

6. Conclusions

In this study, a submerged array jet cooling device for new electric vehicles is designed, and the heat transfer and flow characteristics of jet cooling are simulated by using deionized water as the cooling medium using Fluent software. Orthogonal tests of the main factors affecting the cooling effect are designed and completed. The influence trend of the spacing before and after optimization on the overall flow field fluidity is analyzed. The experimental platform of array jet cooling was built to verify the cooling effect of the optimal spacing value, and the design and optimization of jet cooling device for lithium battery of new electric vehicles are completed, the main conclusions are as follows:

(1) A submerged array jet cooling device is designed based on the 18650 lithium battery as the research object. The nozzle diameter, jet height, transverse and longitudinal jet spacing are selected as the influencing factors, and the maximum temperature, temperature difference, system pressure loss, and Nu value on the jet impact surface are selected as evaluation indicators to design and complete the orthogonal test, Fluent software is used to simulate the jet cooling process of the device, the optimal structural parameters determined by range analysis method are $H = 10mm$, $D = 10mm$, with the transverse jet spacing range of 34-500 mm and the longitudinal jet spacing of 34 mm.

(2) Through particle swarm optimization, under the condition of $H/D = 1$, the optimal value of spacing is $L_1 = 42.6mm$, $L_2 = 34mm$. Combined with the flow velocity cloud chart, the influence trend of the spacing value before and after optimization on the overall flow field fluidity is analyzed.

(3) Building an array jet cooling experimental platform, the experimental results show that when $Re < 1100$, the cooling effect with $L_1/D = 4.26$ is the best, and the cooling uniformity is better at low flow rates. When the flow rate reaches $1.5L/min$, it is not possible to improve heat transfer efficiency by increasing the flow rate. The experimental results show that the flow rate is optimal between $1 - 1.5L/min$. The cooling effect of the optimal spacing value is verified, and the design and optimization of jet cooling device for lithium batteries of new electric vehicles is completed.

In the future, the experimental study on the flow characteristics of the submerged array jet cooling will be considered. Meanwhile, in this experiment, there are also some problems such as splashing out after the impact of some jets, which affect the accuracy of the experiment. The optimization of the experimental platform will be considered in the future.

Acknowledgments

This paper belongs to "Major Natural Science Foundation of Anhui Province Universities Project(KJ2021ZD0144)".This article belongs to "Anhui Province First-class Undergraduate

Major Construction Project(2020ylzyjsd02)".This article belongs to "Anhui Institute of Information Technology Youth Research Fund project(22QNJJKJ008)".

REFERENCES

[1] *Lu M, Zhang X, Ji J, et al.* Research progress on power battery cooling technology for electric vehicles. Journal of Energy Storage, 2020, 27: 101155.

[2] *Singh L K, Kumar R, Gupta A K, et al*. Computational study on hybrid air-PCM cooling inside lithium-ion battery packs with varying number of cells. Journal of Energy Storage, 2023, 67: 107649.

[3] *Talele V, Patil M S, P nchal S, et al.* Battery thermal runaway propagation time delay strategy using phase change material integrated with pyro block lining: Dual functionality battery thermal design. Journal of Energy Storage, 2023, 65: 107253.

[4] *Thakur A K, Sathyamurthy R, Velraj R, et al.* A state-of-the art review on advancing battery thermal management systems for fast-charging. Applied Thermal Engineering, 2023, 226: 120303.

[5] *Kirad K, Chaudhari M.* Design of cell spacing in lithium-ion battery module for improvement in cooling performance of the battery thermal management system. Journal of Power Sources, 2021, 481: 229016.

[6] *Kaood A, Elhagali I O, Hassan M A*. Investigation of high-efficiency compact jet impingement cooling modules for high-power applications. International Journal of Thermal Sciences, 2023, 184: 108006.

[7] *Ruhani B, Abidi A, Hussein A K, et al*. Numerical simulation of the effect of battery distance and inlet and outlet length on the cooling of cylindrical lithium-ion batteries and overall performance of thermal management system. Journal of Energy Storage, 2022, 45: 103714.

[8] *Li X, Zhao J, Duan J, et al.* Simulation of cooling plate effect on a battery module with different channel arrangement. Journal of Energy Storage, 2022, 49: 104113.

[9] *Mehmandoosti M M, Kowsary F.* Artificial neural network-based multi-objective optimization of cooling of lithium-ion batteries used in electric vehicles utilizing pulsating coolant flow. Applied Thermal Engineering, 2023, 219: 119385.

[10] *Garg A, Liu C, Jishnu A K, et al.* A Thompson sampling efficient multi-objective optimization algorithm (TSEMO) for lithium-ion battery liquid-cooled thermal management system: study of hydrodynamic, thermodynamic, and structural performance. Journal of Electrochemical Energy Conversion and Storage, 2021, 18(2).

[11] *Duan J, Zhao J, Li X, et al.* Modeling and analysis of heat dissipation for liquid cooling lithium-ion batteries. Energies, 2021, 14(14): 4187.

[12] *Shahid S, Agelin-Chaab M.* Development of hybrid thermal management techniques for battery packs - ScienceDirect. Applied Thermal Engineering, 2021.

[13] *Lu M, Zhang X, Ji J, et al*. Research progress on power battery cooling technology for electric vehicles. Journal of Energy Storage, 2020, 27(Feb.):101155.1-101155.16.

[14] *Fanfei Bai, Wenji Song, Mingbiao Chen, et al*. Statues quo of research on Li-ion battery thermal management system. Battery bimonthly, 2016(3):4.

[15] *Ruibo Yang*. An Investigation on heat transfer and flow characteristics of confined and submerged jet array impingement on pin-fin heat sinks. Beijing University of Technology, 2010.

[16] *Hai Li, Zhiguo Tang, Qin Gao, et al*. Analysis of heat transfer characteristics of an air jet cooling a conical heat sink. Journal of university of science and technology of China,2020,50(05):551-558.

[17] *Lu Liu*. Simulation of thermal environment control of power lithium battery packs by jet cooling. Zhongyuan University Of Technology,2017.

[18] *Salamah S A, Kaminski D A*. Modeling of turbulent heat transfer from an array of submerged jets impinging on a solid surface. Numerical Heat Transfer, Part A: Applications, 2005, 48(4): 315-337.

[19] *Jiaying Yu, Ziquan Liu*. Optimization of transmission network maintenance schedule based on improved particle swarm algorithm. Guangdong electric powert, 2020, 33(09): 100-107.

[20] *Tran T H, Harmand S, Desmet B, et al*. Experimental investigation on the feasibility of heat pipe cooling for HEV/EV lithium-ion battery. Applied Thermal Engineering, 2014, 63(2):551-558.

[21] *Ke Zeng*. Experimental investigation on heat transfer performance of Nanofluids in a single nozzle free impinging jet. Dalian University of Technology,2016.